Cyclic anoxia and organic rich carbonate sediments within a drowned carbonate platform linked to Antarctic ice volume changes

Swart, Peter K.; Blättler, Clara L.; Nakakuni, Masatoshi; Mackenzie, Greta J.; Betzler, Christian; Eberli, Gregor P.; Reolid, Jesus; Alonso-García, Montserrat; Slagle, Angela L.; Wright, James D.; Kroon, Dick; Reijmer, John J.G.; Hui Mee, Anna L.; Young, Jeremy R.; Alvarez-Zarikian, Carlos A.; Bialik, Orr M.; Guo, Junhua Adam; Haffen, Sebastian; Horozal, Senay; Inoue, Mayuri

published in
Earth and Planetary Science Letters
2019

DOI (link to publisher)
10.1016/j.epsl.2019.05.019

document version
Publisher's PDF, also known as Version of record

Earth and Planetary Science Letters 521 (2019) 1–13

Contents lists available at ScienceDirect

Earth and Planetary Science Letters

www.elsevier.com/locate/epsl

Cyclic anoxia and organic rich carbonate sediments within a drowned carbonate platform linked to Antarctic ice volume changes: Late Oligocene-early Miocene Maldives

Peter K. Swart [a], Clara L. Blättler [b], Masatoshi Nakakuni [c], Greta J. Mackenzie [a], Christian Betzler [d], Gregor P. Eberli [a], Jesus Reolid [e], Montserrat Alonso-García [f,g,1], Angela L. Slagle [h], James D. Wright [i], Dick Kroon [j], John J.G. Reijmer [k], Anna L. Hui Mee [a], Jeremy R. Young [l], Carlos A. Alvarez-Zarikian [m], Orr M. Bialik [n], Junhua Adam Guo [o], Sebastian Haffen [p], Senay Horozal [q], Mayuri Inoue [r], Luigi Jovane [s], Luca Lanci [t], Juan Carlos Laya [u], Thomas Lüdmann [d], B. Nagender Nath [v], Kaoru Niino [w], Loren M. Petruny [x], Santi Dwi Pratiwi [y], Xiang Su [z], Craig R. Sloss [x], Zhengquan Yao [aa,ab]

[a] Department of Marine Geosciences, RSMAS, University of Miami, Miami FL 33149, USA
[b] Department of the Geophysical Sciences, University of Chicago, Chicago IL 60637, USA
[c] Department of Environmental Engineering for Symbiosis, Soka University, 1-236 Tangi-cyo, Hachioji-shi Tokyo 192-0003, Japan
[d] Institute of Geology, CEN, University of Hamburg, Bundesstrasse 55, Hamburg 20146, Germany
[e] Departamento de Estratigrafía y Paleontología, Universidad de Granada, Avd. De la Fuente Nueva S/N, 18071, Granada, Spain
[f] Instituto Portugues do Mar e da Atmosfera (IPMA), Rua Alfredo Magalhães Ramalho, 6, 1495-006 Lisboa, Portugal
[g] Centro de Ciencias do Mar (CCMAR), Universidade do Algarve, 8005-139 Faro, Portugal
[h] Lamont-Doherty Earth Observatory, Columbia University, Borehole Bldg. 61 Route 9W, Palisades NY 10964, USA
[i] Department of Geological Sciences, Rutgers, The State University of New Jersey, 610 Taylor Road, Piscataway NJ 08854-8066, USA
[j] School of GeoSciences, University of Edinburgh, Grant Institute, The King's Buildings, James Hutton Road, Edinburgh EH9 3FE, UK
[k] Geoscience Department, College of Petroleum Engineering & Geosciences, King Fahd University of Petroleum & Minerals, Dhahran 31261, Saudi Arabia
[l] Department of Earth Sciences, University College London, Gower Street, London WC1E 6BT, UK
[m] International Ocean Discovery Program, Texas A&M University, Discovery Drive, College Station TX 77845, USA
[n] Dr. Moses Strauss Department of Marine Geosciences, The Leon H. Charney School of Marine Sciences, University of Haifa, Carmel 31905, Israel
[o] Department of Geological Sciences, California State University Bakersfield, 9001 Stockdale Highway, Bakersfield, CA 93311, USA
[p] GeoRessources lab., UMR 7359, Ecole Nationale Supérieure de Géologie, Université de Lorraine, CNRS, CREGU, 2 Rue du Doyen Marcel Roubault, Vandoeuvre-les-Nancy, F-54501, France
[q] Petroleum and Marine Research Division, Korea Institute of Geoscience & Mineral Resources (KIGAM), Gwahang-no 124, Yuseong-gu, Daejeon 305-350, Republic of Korea
[r] Graduate School of Natural Science and Technology, Okayama University, 3-1-1 Tsushima-naka 700-8530, Japan
[s] Instituto Oceanográfico da Universidade de São Paulo, Praça do Oceanográfico, 191, São Paulo, SP 05508-120, Brazil
[t] Department of Pure and Applied Science, University of Urbino, Via S. Chiara 27, 61029 Urbino, Italy
[u] Department of Geology and Geophysics, Texas A&M University, Mail Stop 3115, College Station TX 77843-3115, USA
[v] Geological Oceanography Division, CSIR-National Institute of Oceanography, Dona Paula Goa 403004, India
[w] Graduate School of Science and Engineering, Yamagata University, 1-4-12 Kojirakawa-machi, Yamagata City 990-8560, Japan
[x] Earth and Environmental Sciences, University of Technology Queensland, R-Block 317, 2 George Street, Brisbane, Queensland 4001, Australia
[y] Department of Geosciences, Geological Engineering Faculty, Universitas Padjadjaran, Jl. Raya Bandung Sumedang Km. 21, Jatinangor 45363, Indonesia
[z] Key Laboratory of Ocean and Marginal Sea Geology, South China Sea Institute of Oceanology, Chinese Academy of Sciences, Guangzhou 510301, PR China
[aa] Department of Marine Geology, First Institute of Oceanography (FIO) State Oceanic Administration (SOA), #6 Xian Xia Ling Road, Qingdao, Shandong Province 266061, PR China
[ab] Laboratory for Marine Geology, Qingdao National Laboratory for Marine Science and Technology, Qingdao, PR China

ARTICLE INFO

Article history:
Received 17 May 2018
Received in revised form 4 April 2019
Accepted 11 May 2019
Available online 14 June 2019
Editor: T. Lyons

ABSTRACT

This paper reports on the newly discovered occurrence of thick sequences (~100 m) of Late Oligocene and Early Miocene (~24.9 to ~20 Ma) interbedded organic-rich sediments (sapropels) and pelagic (organic poor) carbonates at Sites U1466 and U1468 drilled in the Maldives archipelago during the International Ocean Discovery Program (IODP) Expedition 359. This occurrence is unusual in that this sequence is located > 1000 m above the surrounding ocean floor within an inter-atoll basin and

E-mail address: Pswart@rsmas.miami.edu (P.K. Swart).
[1] Now at University of Salamanca, Dept. of Geology, Pza. de los caídos s/n, 37008 Salamanca, Spain.

https://doi.org/10.1016/j.epsl.2019.05.019
0012-821X/

Keywords:
sapropels
anoxia
sea level
carbonate platforms

not linked to any known global oceanic events. Total organic content reaches as high as 35% in the darker layers, while the interbedded carbonates have concentrations of less than 0.1%. Trace elements characteristic of anoxic waters, such as Mo, V, Cr, U, and Pb, correlate positively with concentrations of organic carbon. Nitrogen isotopic data show no evidence that the intervals of high total organic carbon are related to enhanced productivity driven by upwelling. Instead, high organic carbon is associated with intervals of anoxia. We propose that sea-level fluctuations linked to changes in Antarctic ice volume restricted exchange with the open ocean causing bottom waters of the inter-atoll basin to become anoxic periodically. The architecture of the platform at the end of the Oligocene, combined with the global sea-level highstand, set the stage for orbitally-driven sea-level changes producing cyclic deposition of sapropels. The proposed mechanism may serve as an analogue for other occurrences of organic carbon-rich sediments within carbonate platform settings.

1. Introduction

Organic-rich deposits are abundant in the geological record (Algeo, 2004; Arthur, 1979; Jenkyns, 2010; Sageman et al., 2003; Schlanger and Jenkyns, 1976). Whilst many ancient examples are thought to be related to global anoxic events, there are a few examples associated with the development of carbonate platforms (Gardner et al., 2013; Koster et al., 1988) and isolated basins (Emeis and Weissert, 2009; Lyons, 1991; Peterson et al., 1991), where restricted ventilation or enhanced productivity led to the preservation of total organic carbon (TOC). Here, we report on the newly discovered occurrence of a sequence of alternating organic-rich and organic-poor sediments from International Ocean Discovery Program (IODP) Sites U1466 and U1468 in the Maldives Inner Sea (Indian Ocean), examining the possible conditions that led to the formation of this unusual deposit in an inter-atoll basin through geochemical and sedimentological analyses. We also link this depositional system to paleoceanographic changes associated with Antarctic ice volume changes, and suggest that the inter-atoll environment of the Maldives may serve as an analogue system for other known organic-rich deposits with previously unclear origins.

1.1. Background

This study deals with samples from two cores from the Maldives recovered during Expedition 359 of the International Ocean Discovery Program (IODP) (Betzler et al., 2016a). These sediments comprise a ∼3 km thick shallow water and hemipelagic carbonate succession (Aubert and Droxler, 1992) that formed on a lower Paleogene (60–50 Ma) volcanic basement (Duncan and Hargraves, 1990). Although the primary aim of drilling during IODP Expedition 359 was to examine the timing of the South Asian Monsoon, which commenced at 12.9 Ma (Betzler et al., 2016a; Betzler et al., 2018) and coincided with the expansion of the oxygen minimum zone, deeper drilling revealed a ∼100 m section (20–23 Ma) of interbedded hemi-pelagic sediments rich in organic carbon at Sites U1466 and U1468 (Fig. 1). These sediments are the focus of this study.

2. Methods

Samples were taken from every dark layer and the intervening light colored layers between ∼700 and 800 mbsf at Site U1466 and between ∼720 and 805 mbsf at Site U1468. High-resolution sampling was conducted in two core sections, U1466B-56R-1W and U1468A-105X-1W, where 2 cm^3 samples were taken at ∼2 cm intervals (Fig. 2).

2.1. Organic $\delta^{13}C$ and $\delta^{15}N$ values and acid-insoluble material

Co-occurring sedimentary organic material was isolated via dissolution in 5% HCl acid following the method described in Oehlert et al. (2012). The residual organic carbon was combusted in a Costech ECS 4010 (Costech Analytical Technologies, Inc.). Water was removed and oxygenated species of nitrogen reduced to N_2 using a Cu furnace held at 600 °C in the standard manner. For C and N isotopic measurements, the CO_2 and N_2 gases produced were transferred to a continuous flow stable isotope ratio mass spectrometer (Thermo Delta V Advantage). The $\delta^{13}C$ and $\delta^{15}N$ values of the samples are reported relative to the V-PDB (Vienna Pee Dee Belemnite) scale and atmospheric nitrogen respectively. The V-PDB scale for organic carbon is defined by the $\delta^{13}C$ value of graphite (USGS24) = −16.05‰ versus V-PDB (Coplen et al., 2006). Within each run (typically 50 samples), a glycine and secondary standard were analyzed every ten samples. The reproducibility of $\delta^{13}C$ and $\delta^{15}N$ values of the standards was ±0.1 and ±0.3‰ respectively.

2.2. Insoluble residue and total organic carbon

Weights and percentages of insoluble residue and TOC were analyzed and calculated following the methods of Oehlert et al. (2012). The standard deviation of these analyses is 0.4 wt% based upon repeated analyses of glycine (n=54).

2.3. Inductively coupled plasma mass spectrometry

Samples from Core Section U1466B-56R-1W were analyzed for a range of major and trace elements (Li, Na, Mg, Al, K, Ca, Ti, V, Cr, Mn, Fe, Sr, No, Cd, Pb, Th, and U) using a quadrupole inductively coupled plasma mass spectrometry (ICP-MS) using Thermo iCAP-Q at Princeton University. The method thoroughly dissolved the carbonate phase and partially dissolved other mineral phases and organic matter so the values analyzed represent a maximum value for the carbonate phase and a minimum for the bulk sample. Approximately 10 to 25 mg samples of bulk sediment were weighed out directly into clean, acid-washed Teflon beakers. The samples were dissolved by adding 5 mL of concentrated (∼16 N) distilled nitric acid, capping the beakers, and heating them at ∼75 °C for over 12 h. The beakers were then opened and dried down, and an additional 2 mL of concentrated nitric acid was added and dried down. The samples were then redissolved in 5 mL of 2% nitric acid. All mineral components appeared to be dissolved, although some brown detritus resembling remnant organic matter sometimes remained. After centrifugation, the clear supernatant was diluted up to 200x to yield solutions of approximately 10 ppm Ca. Trace element analyses were performed with matrix-matched standards at approximately 10 ppm Ca and with varying trace element concen-

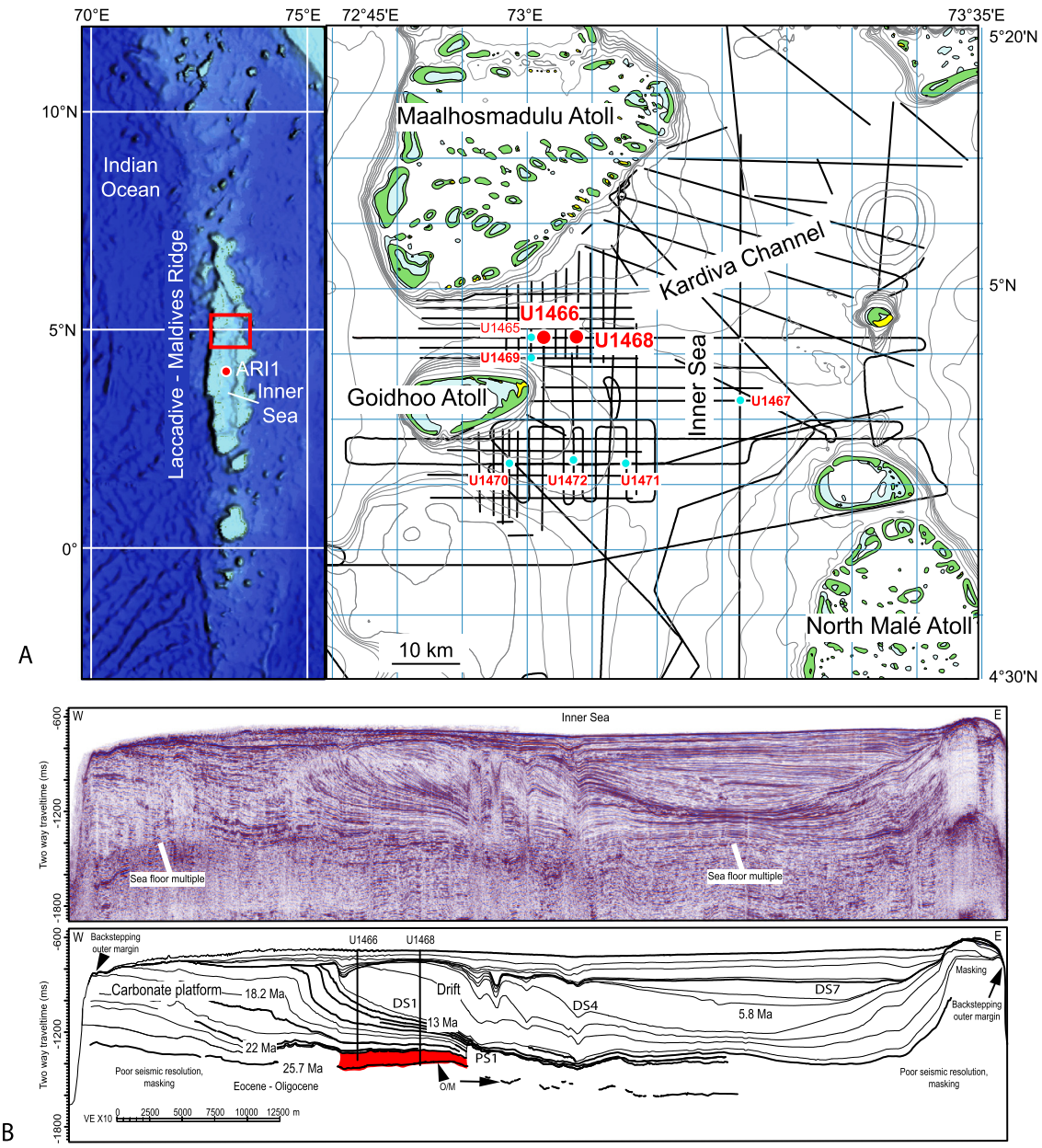

Fig. 1. A) Map showing the location of Sites U1466 and U1468 drilled during IODP Expedition 359. B) Seismic line showing the location and depth of penetration of Sites U1466 and U1468.

trations to bracket those in the samples. Internal errors are better than 3% (RSD).

2.4. X-ray fluorescence

The X-ray fluorescence (XRF) scans were measured at the Ocean Drilling and Sustainable Earth Science (ODASES) XRF scanning facility at the IODP Gulf Coast Repository (GCR) in College Station, Texas (USA) using a third generation AvaaTech XRF scanner configured to analyze split sediment core halves for elements between Mg and U in the periodic table (Lyle and Backman, 2013). The data were acquired with a Canberra X-PIPS Silicon Drift Detector (SDD) with 150 eV X-ray resolution at 5.9 keV and a Canberra Digital Spectrum Analyzer model DAS 1000. The X-ray source was an Oxford Instruments 100 W Neptune X-ray tube with a rhodium (Rh) target. Raw spectral data were processed using the Canberra WINAXIL software package to produce elemental intensity data. The dual slit system was set to provide down-core spatial resolution of 10 mm and cross-core spatial resolution of 12 mm. The system was set to perform three consecutive runs of the same section, the first one at 9 kV, 0.25 mA and 6 s, the second one at 30 kV, 1.25 mA and 6 s, and a third at 50 kV, 2 mA, and 40 s. The elements of interest in the first scan were Ba, Ca, Cr, Fe, K, Mg, Mn, and S, in the second were Br, Mo, and Pb, and Cd in the third. Each core section was removed from refrigeration at least 2 h before scanning and scraped to clean and smooth the core surface. The split core surface was covered with 4 µm thick Ultralene plastic film to prevent contamination of the X-ray detector. Measurements were taken at 3 cm intervals whenever possible. Because measurements cannot be performed if the sediment presents cracks or an uneven surface some measurements were skipped or shifted to the nearest suitable area. In addition, Core Sections U1466B-56R-1W and 2W were analyzed at 2 cm resolution. In order to evaluate the reliability of the analysis of certain elements (Fe, Al, Sr, Si K, Ca, Br, Mo, and Ba) a companion study (Kunkelova et al., 2018) analyzed samples of pressed pellets using

Fig. 2. Core photograph of dark and light layers from Core Sections A) U1466B-56R-1 & 2, and B) U1468A-105X-1.

a fully quantitative conventional XRF method. That study measured 67 samples from Cores 359-U1467C-4H to −6H on a conventional XRF instrument in Edinburgh with the same pellets measured on the AvaaTech XRF core scanner in College Station, Texas. For these, 1 g aliquots of core material were ground in an agate mortar and pestle and then pressed into 1 cm diameter pellets using a pellet press operating at a pressure of 2 t/cm^2. Pellets were analyzed on a Philips PW2404 XRF spectrometer with a Rh-anode X-ray tube. Corrections for matrix effects on the intensities for major element lines were made using theoretical alpha coefficients calculated using Philips software (Reynolds, 1963). Intensities of the longer-wavelength trace element lines were corrected for matrix effects using alpha coefficients based on major element concentrations. For other trace elements, matrix corrections were applied using the Rh K alpha Compton scatter line as an internal standard. Line overlap corrections were applied using synthetic standards. The spectrometer was calibrated with 15 USGS and CRPG standards using the values given in Govindaraju (1994).

2.5. Inorganic stable carbon and oxygen isotopes

Carbonate materials were reacted with phosphoric acid using a common acid bath at 90 °C and the CO_2 released analyzed using a dual-inlet mass spectrometer (Finnigan-MAT 251) at the University of Miami. The CO_2 gas was calibrated using NBS-19 (National Bureau of Standards) and reported relative to V-PDB using the conventional notation. Replicate analyses yielded a precision < 0.1‰ for both $\delta^{13}C$ and $\delta^{18}O$ values.

2.6. Fatty acids

In intervals with high organic content, sediment samples from Hole U1466B were obtained to analyze fatty acids. Fatty acids were analyzed using an on-line TMAH (tetramethylammonium hydroxide) thermochemolysis. Individual finely powdered and dried sediment samples (∼14 mg) were placed in pyrofoil (foil for pyrolysis) and TMAH reagent (97%, Sigma-Aldrich Co., 25 wt.% methanol; 40 µL) was added. After methanol was evaporated to dryness, the pyrofoil was wrapped and set into a Curie point pyrolyzer (JHP-3: Japan Analytical Industry Co.) and heated at 315 °C for 20 s. The resulting TMAH products were introduced into a GC column (DB-5 ms, 30 m x 0.32 mm i.d.; 0.25 µm film thickness) and analyzed by GC mass spectrometry (5975 C; Agilent Technologies Co.).

2.7. Downhole logging

Natural gamma radiation (NGR) and electrical resistivity were measured throughout the interval of organic-rich sapropels and organic-poor carbonates at Site U1468 during Expedition 359 through wireline borehole logging. Downhole logging data were collected at 30 cm resolution with a 15 cm sampling interval using standard shipboard methods employed by IODP, described in detail by Betzler et al. (2016b).

2.8. Statistical methods

Factor analysis was performed using Statistica 8.0 and spectral analysis using MATLAB™ (https://www.mathworks.com). Ages were calculated using the shipboard biostratigraphy (Betzler et al., 2017) and the data were interpolated using a linear method to an interval of 10,000 yrs. Factor analysis was performed on the ICP-MS data and the results normalized using a Varimax method.

2.9. Scanning electron microscopy

Selected samples were examined from Core U1466B-56R in both the dark and light layers. Small rock chips were mounted on aluminum stubs using epoxy resin, sputter coated with gold-palladium and examined using a Zeiss Ultra Plus Field Emission scanning electron microscope (SEM) at the Natural History Museum, London.

3. Results

3.1. Age model

The ages of the sediments were determined by micropaleontologists on the drilling expedition (Betzler et al., 2016b). The integrated nannofossil and planktonic foraminiferal stratigraphy provides a robust biostratigraphic framework for this carbonate sequence representing drowning of an ancient shallow water carbonate platform. Several reliable biostratigraphic events were placed with a high degree of certainty. These include the first occurrence of *Paragloborotalia kugleri*, which indicates the Oligocene/Miocene boundary, and the last occurrence of the late Oligocene species *Sphenolithus ciperoensis*. The description of the sedimentology, age, and various chemical and physical properties can be found in the initial scientific reports (Betzler et al., 2016b) and additional publications (Betzler et al., 2016a; Betzler et al., 2018). Depth versus age plots for the two sites are shown in Fig. 3.

3.2. Sedimentology

The intervals investigated include Unit VII from Site U1466 (715.34-803.61 mbsf) and Unit VI (728.6-817.55 mbsf) from Site U1468. These overlie an Oligocene carbonate platform and a succession of shallow-water deposits (Betzler et al., 2016b) (Fig. 1B). Unit VII from Site U1466 was subdivided into two, with the lower unit (773.71-803.6 mbsf) showing clear manifestations of alternation between white chalks and very dark sediments. The upper portion (715.34-773.71 mbsf) also showed alternations although the contrast was less and diminished with decreasing depth. Based on the core photographs it is likely that the interval in both Sites U1466 and U1468 extends upwards to an age of approximately 20 Ma, albeit with reduced intensity of the darker intervals in the younger sediments. The sediments in these units consist of wackestone, locally and gradually changing into mudstone or packstone and display an alternation of laminated and poorly bioturbated dark intervals with highly to completely bioturbated light intervals (Fig. 4). Sediments in the dark intervals have abundant planktonic foraminifers, fish debris and nannofossils suggesting open marine conditions. The darker layers are finely laminated and locally show scattered discrete small-sized burrows of *Thalassinoides*, *Phycosiphon*, *Palaeophycus*, and *Planolites* and range in thickness from 1 to 25 cm and are intercalated with light wackestone intervals, 5 to 300 cm thick. The sediments in the light intervals are highly bioturbated and contain abundant planktonic foraminifers and nannofossils. The latter are well preserved and diverse and show no consistent assemblage differences between the dark and

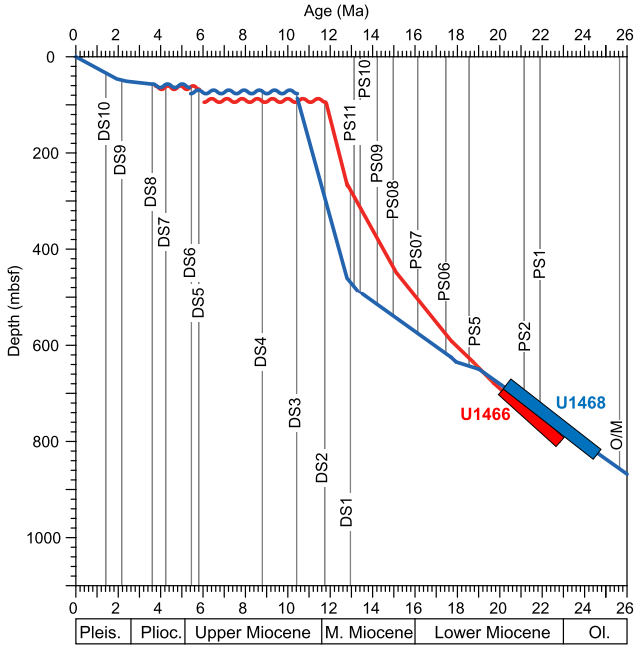

Fig. 3. Age-depth curves for the Sites U1466 and U1468 (modified from Betzler et al. (2018)). The age and depth of the dark and light layers are indicated by the thicker lines.

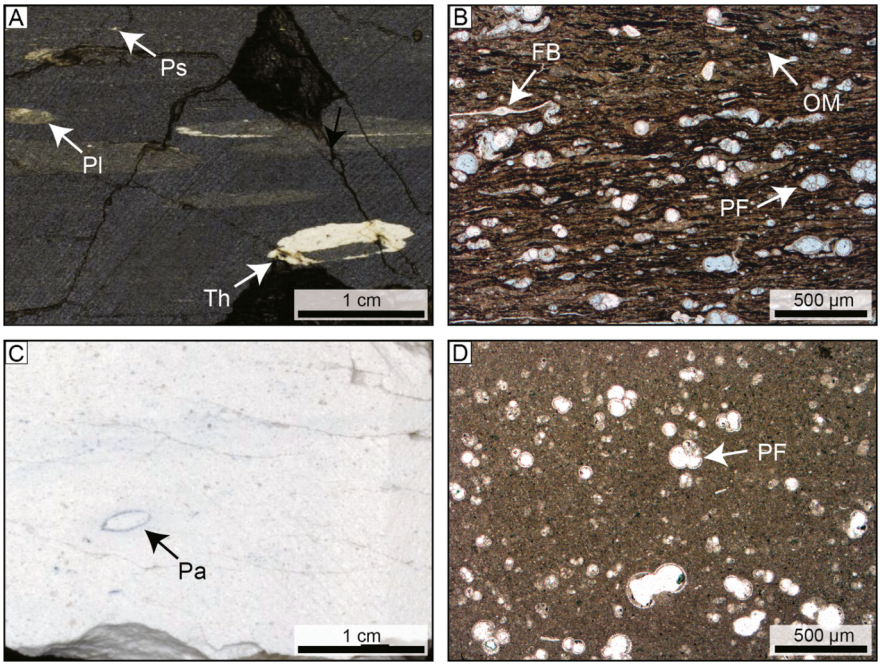

Fig. 4. Facies and components of the dark and light layers. A) Close-up and B) photomicrograph of a dark layer at 790.8 mbsf from Site U1466 (U1466B-56R-1W, 117 cm) showing a wackestone with trace fossils (*Phycosiphon*-Ps, *Planolites*-Pl, and *Thalassinoides*-Th) and allochems (fish bones-FB, planktonic foraminifera-PF, and organic matter-OM). C) Close-up and D) photomicrograph of a light interval at 806.960 mbsf from Site U1468 (U1468A-105X-1W, 76 cm) displaying a wackestone with a burrow of *Palaeophycus* (Pa), and common planktonic foraminifera (PF).

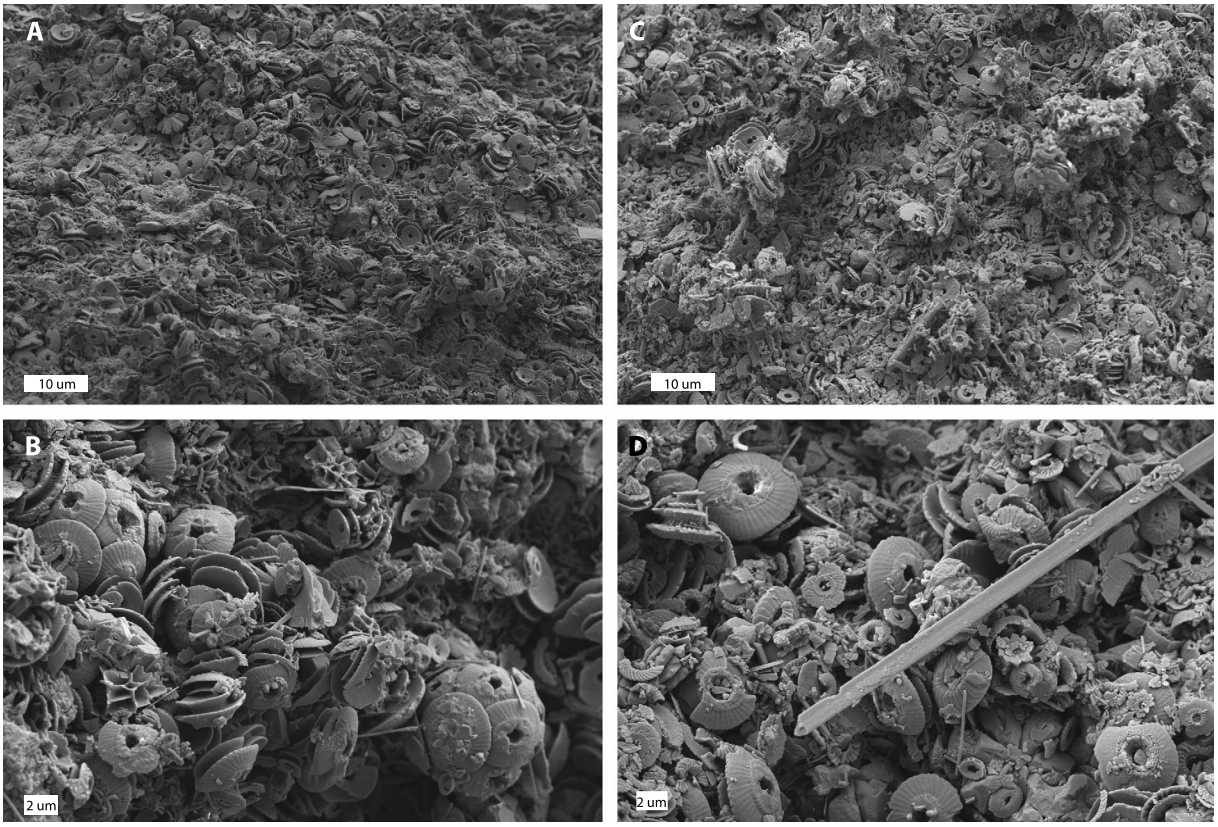

Fig. 5. Scanning electron micrographs of fracture surfaces of sediment samples from a pair of light-dark levels with particularly good nannofossil preservation. A, B) Dark layer, Sample U1466B-56R-1W, 45 cm. The dominant coccolith is *Cyclagelosphaera floridana*, including several coccospheres, *Sphenolithus disbelemnos* is also common (conical nannoliths with honeycomb-like fabric). C, D) Light layer, sample U1466B-56R-1W-35. The dominant coccoliths are *Cyclagelosphaera floridana* (larger circular coccoliths) and *Umbilicosphaera jafari* (smaller circular coccoliths), note also strongly overgrown specimens of *Discoaster deflandrei* (lower right in D).

light intervals (Fig. 5). Fish debris are rare to barren. Underlying the sequence of dark and light layers at Site U1468 is a sequence of shallow-water carbonate sediments representing the drowning of an Oligocene carbonate platform and the formation of the Inner Sea (Betzler et al., 2017).

3.3. Organic content

The darkness of the sediments is related to the TOC of the sediment, which varies between <0.1% within the light layers to as high as 35% in one of the dark layers. The mean TOC ($\pm 1\sigma$) for the dark layers is 8.78±5.6% and 5.77±6.4% for Sites U1466 and U1468, respectively, compared to the light layers which have TOC of 0.73±0.78% and 0.15±0.22%. In both Sites U1466 and U1468, the intervals with the highest TOC are found in sediments between ~22 and 24 Ma (Fig. 6).

3.3.1. Carbon and nitrogen isotopic composition

The mean $\delta^{13}C$ values of the TOC ($\delta^{13}C_{TOC}$) are −20.9‰ at Site U1466 and −22.7‰ at Site U1468; there is no statistically significant variation between the dark and light layers. However, there is a gradual increase in the $\delta^{13}C$ values at both Sites U1466 and U1468 from the base to approximately the top of the interval in which the dark and light layers are found. In Site U1466, the increase in $\delta^{13}C$ values is from −23 to −17‰ while at Site U1468 the $\delta^{13}C$ value increases from −24 to −20‰. Within the zone of dark and light alternations, the $\delta^{15}N$ values of the TOC range from −1 to +2‰ with the organic-rich zones generally expressing more negative $\delta^{15}N$ values (Fig. 7).

3.3.2. Fatty acids

Most of the fatty acids are in the range C_{12} to C_{32}, with C_{14}–C_{18} fatty acids dominant (supplemental material, S1). There is a statistically significant increase in C_{24}–C_{32} fatty acids below ~770 mbsf and the ratio of C_{24}–C_{32} fatty acids to C_{14}–C_{18} fatty acids (long/short ratio) increases towards the base of the dark and light intervals.

3.3.3. C/N ratio

The C/N ratio of the organic material varies between 10 and 20 with no statistically significant differences between the dark and light layers. There appears to be a decrease in the C/N ratio towards the middle of the interval containing the dark and light layers followed by an increase towards the top.

3.4. Carbonate

3.4.1. Oxygen and carbon isotopic composition

Within Core U1466B-56R there is a variation of ~1‰ in the $\delta^{18}O$ values, with more positive values anticipating a concomitant increase in TOC (Fig. 7). The amplitude of these cycles is similar to the early Miocene benthic cycles of $\delta^{18}O$ values in foraminifera noted over the same time interval on Ceara Rise (Zachos et al., 2001). However, overall, the mean $\delta^{18}O$ values of the dark layers (−1.86‰ in Site U1466 and −2.29‰ in Site U1468) are slightly more negative than the light layers (−1.60‰ in Site U1466 and −1.96‰ in Site U1468). The $\delta^{13}C$ values of the carbonate components are more negative within the dark layers compared to the light layers (+0.84‰ vs +1.28‰ in Site U1468; +0.97‰ vs +1.24‰ in Site U1466 ($p < 0.01$)) (Fig. 7).

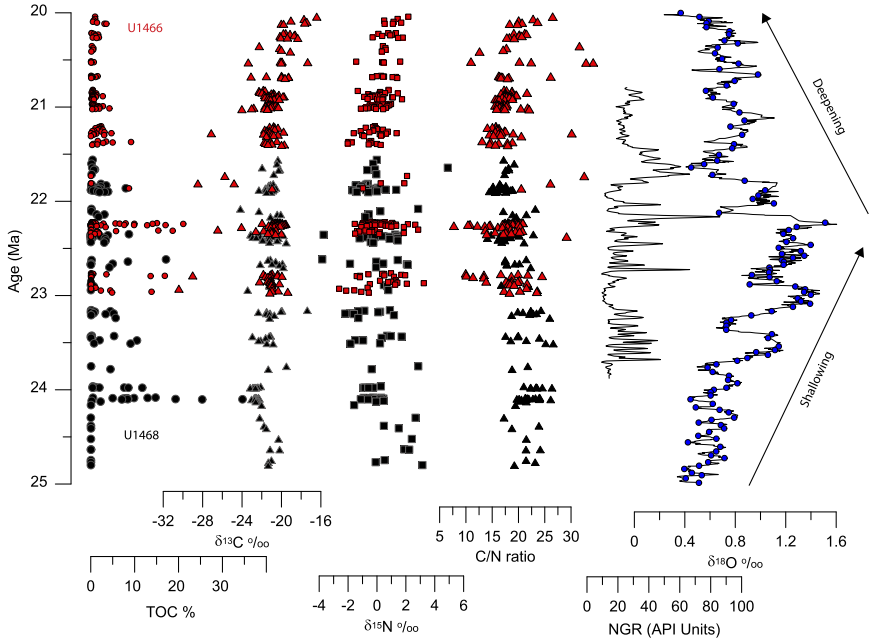

Fig. 6. Changes in the percent organic content, $\delta^{13}C_{OM}$, $\delta^{15}N$ and C/N ratio and NGR (wireline logging data) for Sites U1468 and U1466 between 20 and 25 Ma. Two data points for the C/N ratio from Site U1466 have been omitted because they have values > 60. Wireline data are for Site U1468 only. Site U1468 is shown in the black symbols and Site U1466 with the red symbols. Also shown is the compilation of benthic $\delta^{18}O$ values for the same time period from Zachos et al. (2001). (For interpretation of the colors in the figure(s), the reader is referred to the web version of this article.)

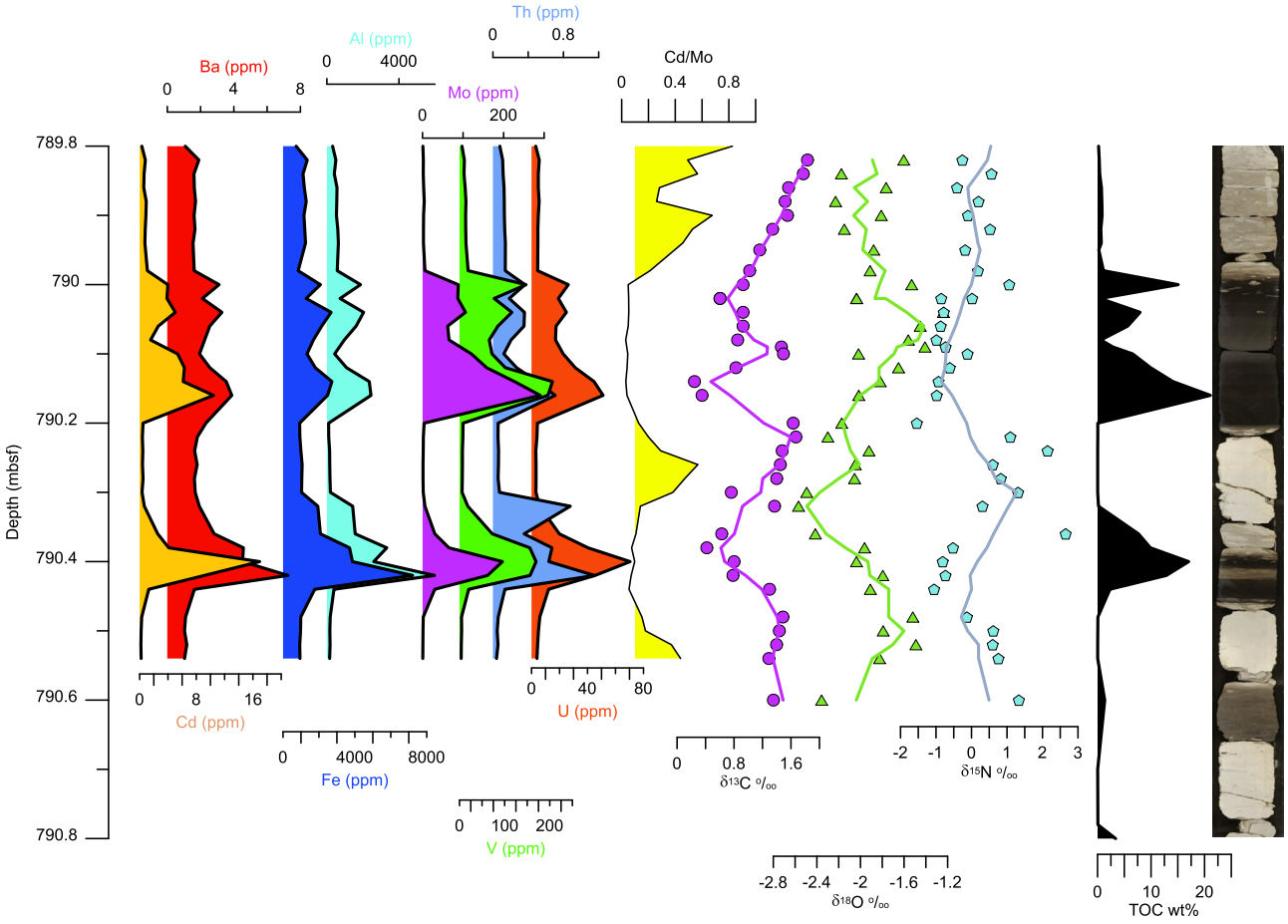

Fig. 7. Changes in the concentration of Cd, Ba, Fe, Al, Mo, V, Th, and U (determined by ICP-MS) compared to the percentage of organic carbon, the $\delta^{18}O$ and $\delta^{13}C$ values of the carbonate and the $\delta^{15}N$ values measured in the TOC in Core Section U1466B-56R-1. The solid line in each graph represents a three-point moving average. All metal concentrations in ppm. Also shown is the Cd/Mo ratio as defined by Sweere et al. (2016). This shows the lowest values which are characteristic of anoxia, within the darker organic-rich layers.

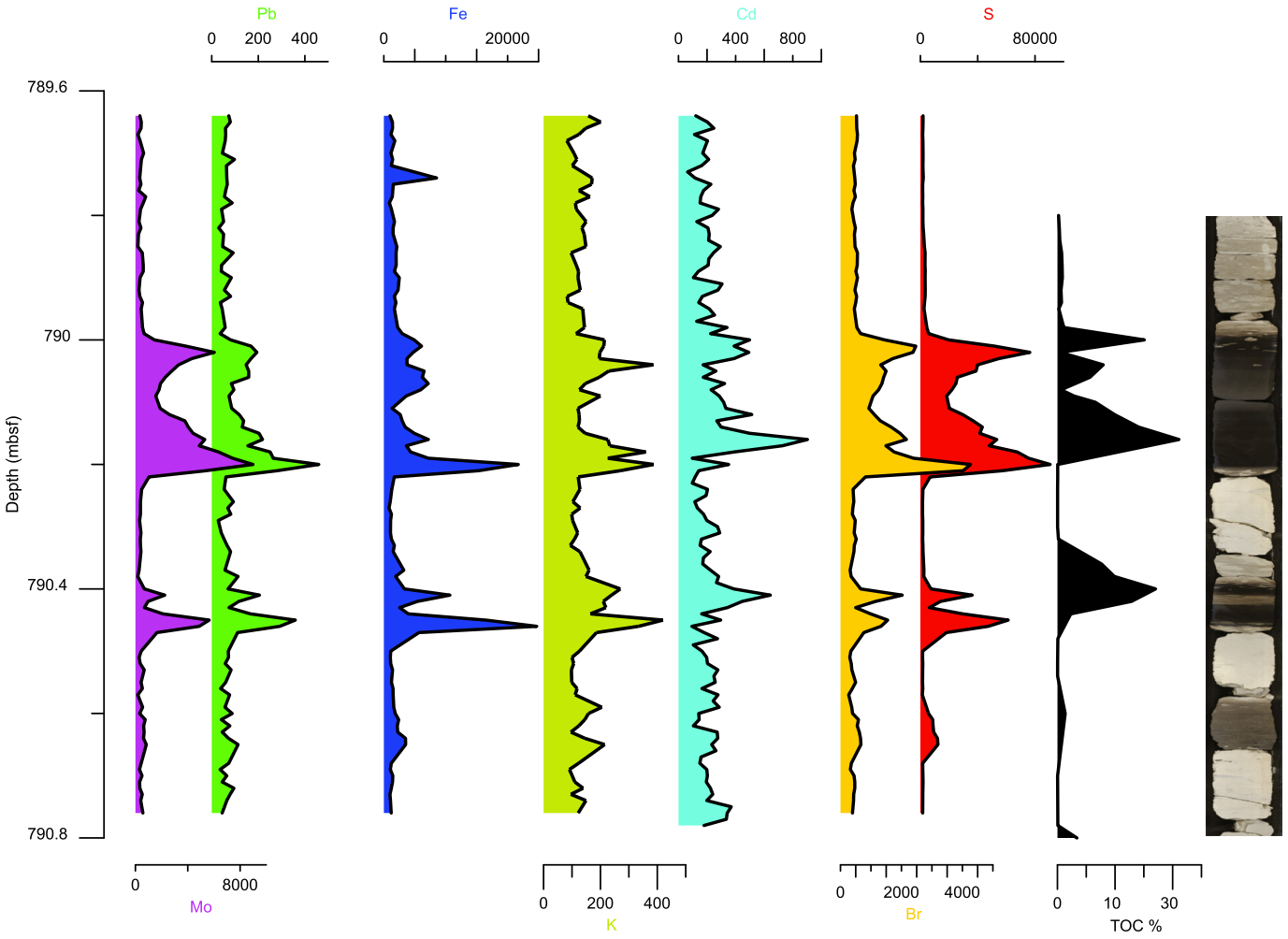

Fig. 8. XRF data from Core Section U1466B-56R-1 showing the variation in redox and dust related elements (Mo, Pb, Fe, K, Cd, Br, & S) associated with the dark and light layers (shown in core photograph). Concentration units for all elements are in counts per second.

3.4.2. Trace elemental analysis

Scanning X-ray fluorescence

The elements Br, Cd, Fe, Mo, S, Pb, and Zn show a strong positive correlation between each other and with the concentration of TOC in the cores (Figs. 8 and 9). Generally, there is a sharp rise in the concentration of trace elements at the base of each dark interval mirroring changes in the 'darkness' of these intervals.

Wet chemical analyses

Samples from Section U1466B-56R-1 were analyzed for a range of elements using ICP-MS. Whilst some of the elements analyzed were the same as those measured using XRF (Ca, Fe, Mo, Pb, and Sr), several others (Cr, Th, U, and V) were only analyzed using ICP-MS and provide important additional information on the redox state and origin of the sediments. The concentration of certain elements (Ca, Fe, Mo, Pb, Al, and Sr) measured using ICP-MS are generally correlated with intensities measured using XRF, albeit with a lag of ~2-4 cm (See supplemental material, S2 for cross plots between XRF and ICP-MS data and discussion). For other elements (Cr, Ba, and Mg) no correlation was observed between the two methods (See supplemental material). Analogous to the XRF data, the concentration of a number of elements (Al, Ba, Cd, Cr, Fe, Li, Mo, Pb, Th, V, and U) were positively correlated with TOC in this core (Fig. 7). Principal component analysis shows a preferential clustering of Al, Cd, Cr, Fe, K, Li, Mo, Pb, Th, U, and V accounting for 54% of the variance (supplemental material, Fig. S3-11).

Comparison to quantitative XRF analyses

Correlation coefficients range from about < 0.1 to ~0.9 with K and Si having the highest values of about 0.9. Elements such as Fe, Si, and Al show R^2 values > 0.8. A full comparison of the results from both methods are included in the supplemental material (S1).

3.4.3. Natural gamma radiation

At all sites, spectral natural gamma radiation (NGR) logs show that the NGR signal is almost entirely the result of variations in the concentration of U, with K and Th contributing only a minor proportion of the total signal (Betzler et al., 2016b). The NGR signal routinely shows a positive correlation with the concentration of TOC ($R^2 = 0.40$, n=88 for Site U1468; $R^2 = 0.36$, n=71 for Site U1466) and can be used to correlate core material with downhole logging data. Based on changes in the downhole NGR signal, between 30 and 35 dark (high TOC) layers were identified between 24 and 21 Ma, only some of which were recovered in cores during drilling. A spectral analysis of NGR data show peaks at ~100 and 50 K yrs (Fig. 10A). Downhole NGR data were not measured below ~800 mbsf at Site U1468 so the oldest section of the interval is not represented.

3.4.4. Electrical resistivity

The electrical resistivity signal obtained from downhole logging is strongly correlated with the gamma radiation signal and was measured as deep as ~822 mbsf at Site U1468; thus the resistivity

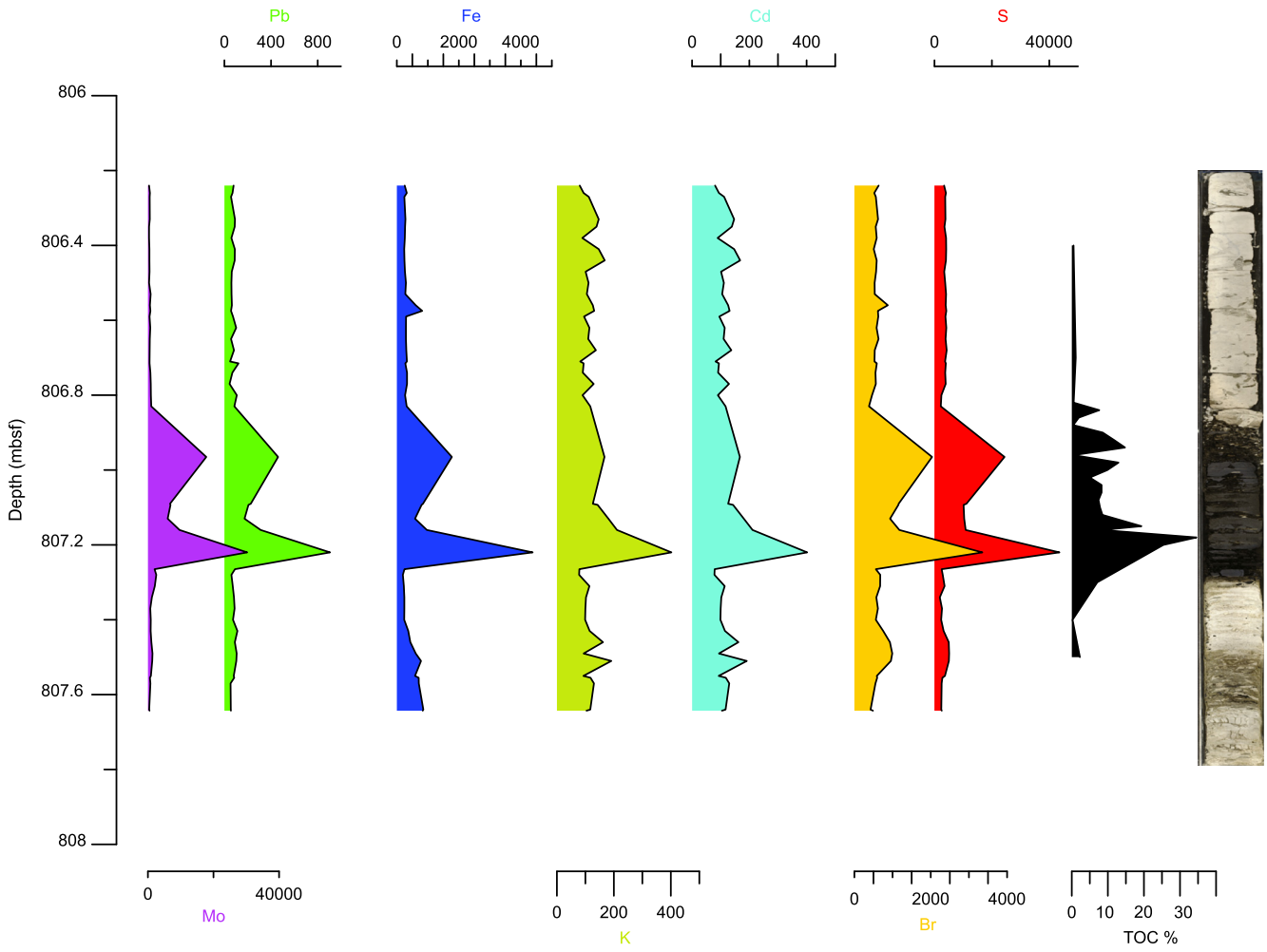

Fig. 9. XRF data from Core Section U1468A-105x-1 showing the variation in redox and dust related elements (Mo, Pb, Fe, K, Cd, Br, & S) associated with the dark and light layers (shown in core photograph). Concentration units for all elements are in counts per second.

data span the full dark and light interval at this site. Resistivity, the inverse of conductivity, is typically used to evaluate porosity and these data indicate that the U-rich, dark layers likely have lower porosity (or less connected pore space and higher resistivity) than the light layers. A spectral analysis of these data (Fig. 10B) show peaks around 120, 80, and 40 K yrs.

4. Discussion

Previous work has shown that a rimmed platform with a protected basin developed in the Maldives during the Early to Late Oligocene transition when shallow-water carbonate production became restricted to narrow bands at the ocean-ward edges, forming a saucer shaped basin perhaps 50-100 m deep (Betzler et al., 2018). The platform drowning at the Oligocene-Miocene transition coincided with a major sea-level rise during the early Miocene with an amplitude of approximately 50 m (Miller et al., 2011) and is perhaps synchronous with platform drowning events recognized in other locations (Mutti et al., 1997). After the drowning there was a gradual decrease in sea level (Zachos et al., 2001) which is coincidental with the development of the sapropels described in this paper.

While many factors can contribute to the origin of the color differences including variations in trace elements such as Fe, it is likely that the major cause of variations in these cores is a consequence of changes in the amount of organic material, with the darker layers, identified simply on a subjective inspection of color, containing an average of between 5.8 and 9.8 wt% compared to 0.16 to 0.73 wt% in the lighter colored intervals. Whilst the presence of abundant oceanic biota suggests that oceanic conditions were prevalent during deposition of both dark and light layers, the darker ones have the characteristics of sediments deposited in anoxic basins including a high TOC (2-39%) and an abundance of redox-sensitive trace elements (Brumsack, 2006; Tribovillard et al., 2006). The occurrence of such layers is normally thought to result from enhanced productivity, enhanced preservation of organic material, dilution of the organic material by inorganic material, or some combination of all of the above.

4.1. Productivity

While an enhanced productivity origin for the high TOC within the darker layers is supported by slightly higher concentrations of nutrient-related elements such as Cd, and to a lesser extent Ba, Cu, and Zn, the interpretation of variations in these elements is not straightforward (Tribovillard et al., 2006) and alternative explanations, such as enhanced input of dust, are also possible. In some instances, higher concentrations of these elements are related to upwelling resulting in higher inputs of nutrients such as nitrate and phosphate (Boyle, 1981; Lea and Boyle, 1991) which in turn drive higher productivity within the water over the platform. However, upwelled waters would have been influenced by denitrification resulting in organic components with relatively positive δ^{15}N values (Altabet and Deuser, 1985). This is contrary to what is

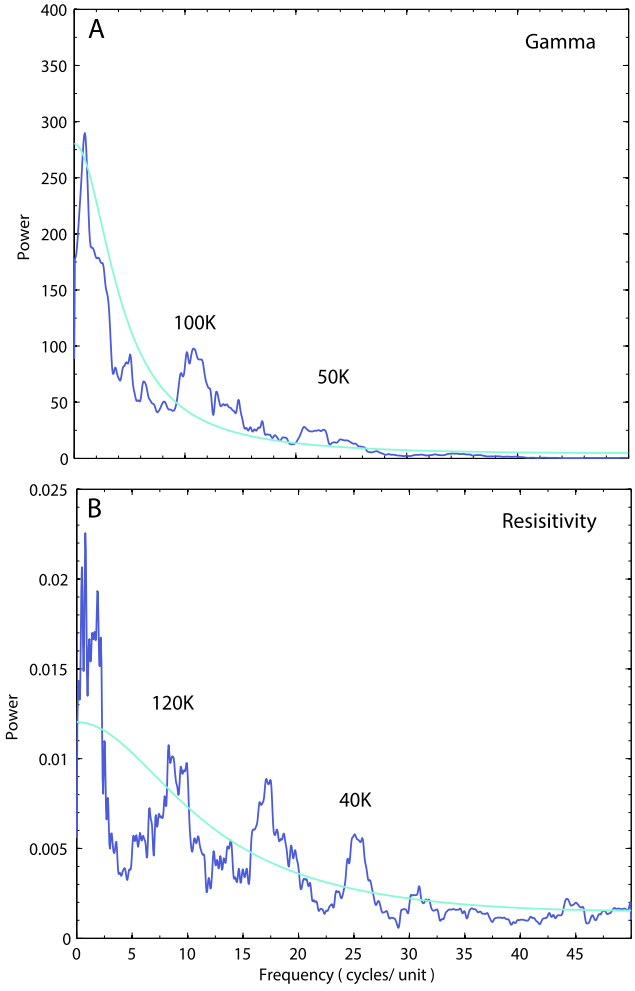

Fig. 10. A) Spectral analysis of natural gamma radiation data obtained from the downhole wireline logging at Site U1468 between a depth of 700 and 800 mbsf. B) Spectral analysis of electrical resistivity data from downhole wireline logging at Site U1468 between a depth of 700 and 820 mbsf. For both gamma radiation and resistivity data, age assignments have been made using shipboard biostratigraphy and have been interpolated to a time interval of 10,000 years. The blue line denotes the 95% significant level.

observed with the organic matter in the dark layers having δ^{15}N values close to 0‰ (Fig. 7). This suggests that nitrogen fixation, rather than upwelled nitrate, was the major source of nitrogen for the organic production. Another potential source of nutrients in the darker layers is atmospheric dust (Figs. 7–9), identifiable as intervals elevated in Al and K. While under coastal conditions fluvial sources might contribute non-carbonate materials, in The Maldives atmospheric deposition would be the primary source. This is supported by work which has shown an increased supply of dust in glacial periods during the past 2 Myrs, variation which is clearly related to Milankovitch periodicity (Kunkelova et al., 2018). In fact the darker layers do have high concentrations of K and Al, suggesting either a constant input of dust combined with a lower sedimentation rate within the darker intervals, or an enhanced dust input during these times. Nitrogen in dust typically has δ^{15}N values close to zero (Knapp et al., 2010) and therefore the values are consistent with the data measured in this study. Lastly, it should be noted that N-fixation needs higher supplies of Fe, an element which is normally low in surface seawater. It has been proposed that such Fe can be supplied from dust and promote nitrogen fixation (Swart et al., 2014). Regardless of the source of nutrients, enhanced productivity should have resulted in more positive δ^{13}C values within the carbonate of the dark layers. In fact, the carbonate within the darker layers possesses more negative δ^{13}C values compared to the light layers, suggesting the darker layers cannot be explained by higher productivity. There were no differences in the $\delta^{13}C_{TOC}$ values between the dark and light layers. Hence, the δ^{13}C values of both the organic and inorganic components tend to discount the enhanced productivity hypothesis as the major control on variability in TOC within the dark and light layers, although it may have been a contributing factor. These considerations as well as an absence of any consistent changes in the nannofossil assemblages between the light and dark layers suggests that any productivity signal was muted (Young et al., 2019).

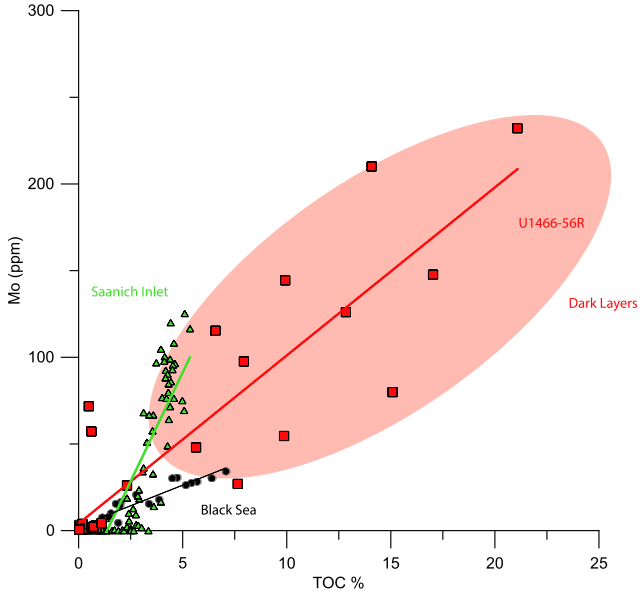

Fig. 11. Data from Core Section U1466B-56R-1 showing the relationship between the concentration of Mo and the TOC (red symbols) relative to similar data published by Algeo and Lyons (2006) from the Black Sea and Saanich Inlet; data for the Black Sea (black circles) and Saanich Inlet (green triangles) are from Algeo and Lyons (2006) and (Francois, 1988) respectively. Data for the dark intervals are highlighted in the oval while the light layers have values of Mo and TOC close to zero.

4.2. Preservation

An enhanced preservation origin for the TOC within the dark layers implies that the bottom waters periodically became anoxic during sediment deposition, thus inhibiting degradation of organic material. This is supported by the higher concentrations of redox sensitive elements such as Mo, V, Th, Cr, and U within these organic-rich layers (Algeo and Lyons, 2006; Tribovillard et al., 2006). Under reducing conditions Mo, V, Cr, and others are quickly adsorbed by Fe and Mn-oxyhydroxides or incorporated into sulfides. As a consequence, while the waters in modern anoxic basins show high concentrations of these elements, they are also scavenged from the bottom waters, leading to an eventual depletion of these elements in poorly ventilated basins. Basins which are very restricted tend to have lower concentrations than those basins with moderate restriction. This situation is well exemplified by Mo which has been widely used as a paleoredox proxy (Algeo and Maynard, 2004; Piper, 1974; Sageman et al., 2003). Variations in the concentration of Mo relative to TOC was studied in a number of modern anoxic basins, including the Cariaco Basin, the Black Sea, Framvaren Fjord, and Saanich Inlet (Algeo and Lyons, 2006). These basins have sedimentary Mo/TOC ratios ranging from ~5 to 50 (x 10^{-4}). By comparison, samples from the darker organic-rich layers of Core U1466B-56R have Mo/TOC ratios of approximately 30, similar to those found in the Cariaco Basin and near the highest ratios found in modern anoxic basins (Fig. 11). Using the correlation be-

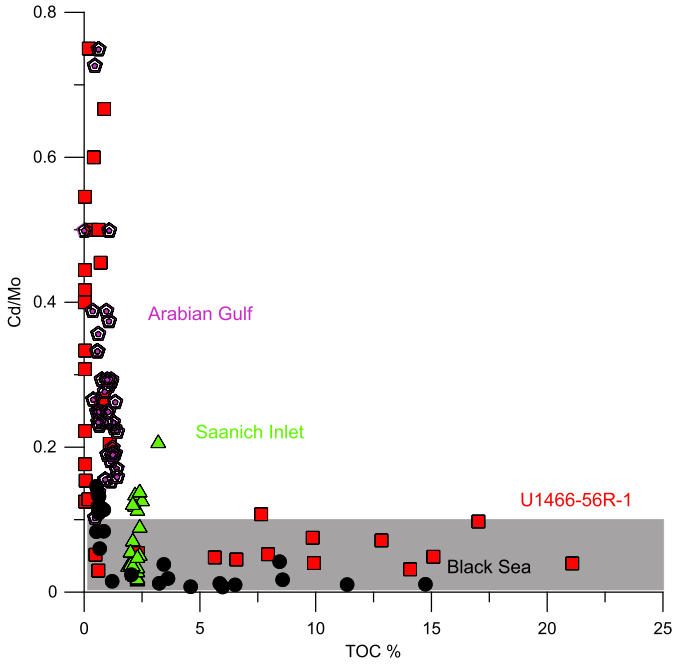

Fig. 12. Plot of the Cd/Mo ratio versus TOC as a distinction between upwelling (Cd/Mo > 0.1) and restricted settings (Cd/Mo <0.1) after the definition of Sweere et al. (2016). Data from the Black Sea (black circles) (Brumsack, 1989), Arabian Sea (purple polygons) (van der Weijden et al., 2006), and Saanich Inlet (green triangles) (Russell and Morford, 2001) shown for comparison. Data from the darker layers from Core U1466B-56R fall below the 0.1 cutoff and support a preservation origin for these intervals.

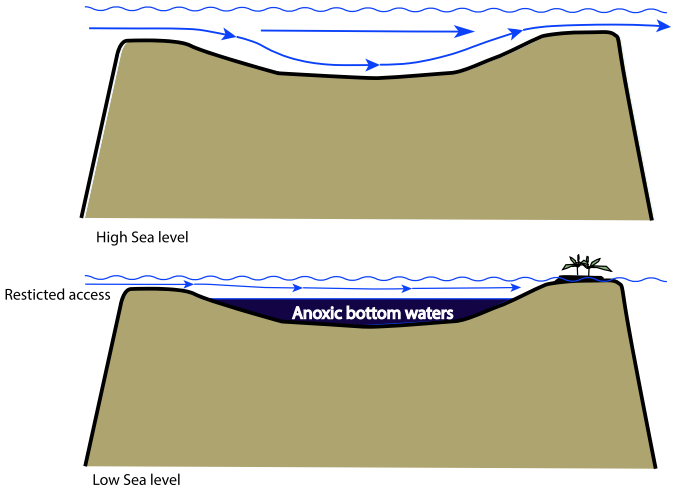

Fig. 13. Cartoon demonstrating how sea level changes could lead to the development of anoxia. In the upper panel the inner-atoll basin is connected to the surrounding ocean and water flows freely into the basin. In the lower panel, sea level has fallen and access to the basin becomes restricted leading to the development of anoxia.

tween Mo/TOC ratios presented by Algeo and Lyons (2006) would suggest a ventilation age for the ancient inner sea of between 10 and 100 yrs, intermediate between basins such as the Black Sea (ventilation age > 500 yrs) and the Saanich Inlet (ventilation age < 2 yrs) (Algeo and Lyons, 2006). Another proxy which has been used to distinguish the roles of productivity and preservation is the Cd/Mo ratio (Sweere et al., 2016). These workers distinguished areas with high organic contents produced by upwelling on the basis of Cd/Mo ratios greater than 0.1 compared to those in which high TOC was a result of preservation. In the data presented in Fig. 7, the Cd/Mo ratios are elevated in the lighter layers (Fig. 12), suggesting that these are influenced by upwelling while the darker layers have Cd/Mo ratios indicative of anoxia (<0.1). While this is consistent with the δ^{15}N values which are elevated in the lighter layers in sediments, the Cd/Mo ratios can be dominated by trends in the trace element composition of the detrital fraction. Hence the principal conclusion which can be drawn here is that the darker layers have low Cd/Mo ratios which strongly support a preservation origin.

4.3. Dilution

The role of sediment dilution has been proposed to account for the alternation of organic-rich and organic-poor layers in some instances (Bohacs, 2005). In order to explore this idea in Core U1466B-54R we can assume a constant flux of Al (presumably derived from dust) as well as a constant input of organic material from the surface ocean.

We then calculate the increase in sedimentation rate needed to dilute the Al from the high concentrations seen in the darker layers to the lower values in the lighter intervals. Consider the dark layer from Core Section U1466B-54R-1, 80-87 cm (Fig. 2) which has an approximate Al concentration of between 2000 and 5000 ppm and a TOC between 12 and 17%. The transition to the overlying lighter zone (Core Sample U1466B-54R-1, 63-73 cm) is marked by a reduction in the Al concentration to 150 ppm and the TOC to 0.03%. While the concentration of Al could be reduced by increasing the rate of sedimentation by between 10-30 times, this would be insufficient to reduce the TOC to that observed. Therefore while sedimentation rate may play a role in causing variations in the preservation of organic material, it is unlikely to have been a major causative factor in controlling the TOC of the sediments in this case.

4.4. Consensus

While based on the variations seen in the concentrations of various trace elements, there appears to be some evidence for enhanced productivity, perhaps driven by input of dust, as well as some role for sediment dilution, it is likely that the principal reason for the elevated TOC is enhanced preservation as a result of anoxia. Such anoxic conditions could have arisen in response to sea-level changes, allowing the bottom waters in the basin to become isolated by virtue of a relatively shallow sill depth connecting the enclosed basin to the surrounding ocean. A similar control has been postulated for the organic-rich sediments in the Cariaco Basin (Peterson et al., 1991), and Black Sea (Lyons, 1991) and it is probably more than coincidental that the Mo/TOC ratios within the dark layers from the Maldives Core U1466B-56R are similar to those found in the Cariaco Basin. A potential model of this mechanism in shown in Fig. 13. Support for this mechanism of sea-level variation driving restriction and enhanced organic matter preservation comes from other paleoceanographic indicators from this time. During the late Oligocene-Early Miocene changes in the volume of the Antarctic ice sheet produced variations of approximately 50 m in sea level, well documented in the benthic (*Cibicides* spp.) oxygen isotope record (Liebrand et al., 2017; Zachos et al., 2001). Such variation is also present in the δ^{18}O values of the carbonate fraction in Core U1466B-56R, which shows oscillations of about 1‰ between the dark and light layers. The changes in TOC tend to lag changes in the δ^{18}O values, as would be expected if sea level were a driving force in the preservation of TOC (Fig. 7). Sea-level control of anoxia is also supported by the spectral analysis of the gamma radiation and electrical resistivity signals obtained from downhole logging. These data reveal the presence of signals approximately coincident with tilt (40 Ky) and eccentricity (100-120 Ky) frequencies (Figs. 10A & B). Higher gamma ray signals are predominantly the result of in-

creased concentration of U; this would correspond to periods of bottom-water anoxia which in our model would be formed during sea-level low stands. Similar spectral frequencies were noted in the Zachos et al. (2001) and Liebrand et al. (2017) datasets. The 20 K frequency was not observed in this study because of the low spatial resolution of the downhole logging data relative to the rate of sediment deposition. We do not see a mechanism such as that proposed for the production of sapropels in the Mediterranean in which increased freshwater input was responsible for the development of anoxia (Emeis and Weissert, 2009; Rossignol-Strick, 1985). In the case of the Maldives there are no major rivers influencing the region, such as in the Mediterranean, and therefore all the freshwater would have to be derived from rainwater. Not only would the volumes of water necessary be unrealistic, but this freshwater would cause the carbonate component to have more negative $\delta^{18}O$ values during the periods of dark layer formation, the opposite of what is observed.

4.5. Changes during the deposition of the 'dark and light' interval

Several observations shed light on the evolution of the light and dark sequences. First, the frequency of the alternations and variations in TOC are much greater in the older portion of the sequence suggesting that the isolation of the basin was much more effective during this time. Hence, later intervals did not experience the same degree of anoxia as evidenced by the lower TOC and the presence of burrows. At the same time the $\delta^{13}C_{TOC}$ values, while not showing significant changes between dark and light layers, show an overall increase from the bottom to the top of the dark and light interval (23.1 to 20 Ma) (Figs 8 & 9). These more negative values may have originated from higher input of terrestrial material at the bottom of the sapropel-bearing interval. Such an interpretation is supported by the relative distribution of short (C_{14}–C_{18}) and long (C_{24}–C_{32}) chain fatty acids (See supplemental material, Fig. S1-1 and S1-2) and changes in the C/N ratio of the TOC. The short chain fatty acids are mainly derived from aquatic organisms such as phytoplankton, while long ones are derived from higher plants (Cranwell, 1974; Ishiwatari et al., 2006; Meyers and Eadie, 1993). The trend within the dark and light intervals at Site U1466 shows a pronounced decrease from the bottom to the top of the interval. This may be a result of an increase in water depth from the late Oligocene to the Early Miocene, meaning that the changes in sea level would be less effective in producing anoxia, or alternatively a reduction in the magnitude of sea-level changes as suggested by the data of Liebrand et al. (2017). At Site U1468 there is a statistically significant decrease in the C/N ratio in this interval, also interpretable as a reduction in the influence of terrestrial plants (Meyers and Eadie, 1993). At Site U1466, the C/N ratio is already close to the value expected for marine TOC throughout, and more positive $\delta^{13}C_{TOC}$ values compared to Site U1468 suggest that the site received less terrestrial TOC.

4.6. Impact of dark and light layers on the global carbon cycle

Numerous studies have noted that there was globally an approximate 0.5‰ increase in the $\delta^{13}C$ values of certain foraminifera coincident with the Oligocene-Miocene boundary (Hodell and Woodruff, 1994; Liebrand et al., 2017; Woodruff and Savin, 1989; Wright and Miller, 1992), although no specific carbon burial event has been identified that coincides with this change. Whilst the direction and the timing of the change is consistent with the increased burial of organic carbon noted in this paper, the amount of carbon theoretically deposited in the Maldives during this time interval is insufficient to induce a global change in the $\delta^{13}C$ value of seawater DIC of 0.5‰. For example, if similar sapropels were present in the Maldives at the same time, then the potential area available for these to form would be ~45,000 km^2. Assuming that 50% of these strata were similar to the dark layers found in this study and that they contained on average 10% organic carbon, then the amount of buried organic carbon, based on a Berner type model (Berner et al., 1983), would be approximately 100 times less than needed to account for the observed change in the global $\delta^{13}C$ value and other processes are therefore necessary to account for the change in $\delta^{13}C$ values, or other sites of organic accumulation must have been active at this time.

5. Conclusions

We have identified the presence of ~100 m thick sequences of organic-rich sediments (sapropels) alternating with organic poor oceanic carbonates in Late Oligocene and Early Miocene strata in the Maldives Archipelago. The organic-rich components contain up to 30% organic carbon and have trace element signatures characteristic of formation within anoxic bottom waters. These alternations occurred within an atoll-like setting over 1000 m above the surrounding ocean basin. Based on stable O and C isotopic variations within the carbonate components as well as spectral analysis of downhole logging data, we propose that these sapropels formed in response to the variations in orbitally induced sea-level fluctuations linked to Antarctic ice volume changes superimposed on a major transgression, which flooded a Late-Oligocene shallow-water carbonate platform. From the initiation of sapropel deposition around 25 Ma, sea level gradually decreased over a period of ~2 Myrs (Fig. 6). Superimposed on this decrease were glacially driven changes which, because of the long term decrease in sea level, were more effective at isolating the inner sea thereby causing the bottom waters to become anoxic and conducive to the preservation of organic material. Toward the end of the sapropel-bearing interval (22.5 – 20 Ma) sea level increased and the isolation of the bottom water became less effective and the intensity of the sapropels diminished. While sea-level induced ventilation has been proposed for the development of anoxia in closed basins such as the Cariaco Basin (Peterson et al., 1991) and Mediterranean (Emeis and Weissert, 2009) leading to the formation of sapropels, subtle changes in sea level might also be responsible for the formation of organic-rich intervals within other carbonate platform settings.

Acknowledgements

The authors would like to thank the crew and technicians of the JOIDES Resolution. Analyses in Miami were supported by A. Saied. D. Houpt and M. Schoemann are acknowledged for assistance during XRF scanning at IODP Gulf Coast Repository. Support for MAG was provided by the Portuguese National Science and Technology Foundation (SFRH/BPD/96960/2013 and UID/Multi/04326/2013). Fatty acid analyses were supported by K. Takehara, S. Yamamoto, and the JAMSTEC IODP After Cruise Research Program (Exp. 359). The SEM analyses were supported by the Natural History Museum, London and funding from UKIODP (NE/N014049/1). DK acknowledges support by the NERC (3148). Support for U.S. participants was provided by the IODP U.S. Science Support Program (NSF OCE1450528). Support for G. Mackenzie was provided by the Comparative Sedimentology Laboratory. The manuscript was improved through the comments of three reviewers.

Appendix A. Supplementary material

Supplementary material related to this article can be found online at https://doi.org/10.1016/j.epsl.2019.05.019.

References

Algeo, T.J., 2004. Can marine anoxic events draw down the trace element inventory of seawater? Geology 32, 1057–1060.

Algeo, T.J., Lyons, T.W., 2006. Mo-total organic carbon covariation in modern anoxic marine environments: implications for analysis of paleoredox and paleohydrographic conditions. Paleoceanography 21.

Algeo, T.J., Maynard, J.B., 2004. Trace-element behavior and redox facies in core shales of upper Pennsylvanian Kansas-type cyclothems. Chem. Geol. 206, 289–318.

Altabet, M.A., Deuser, W.G., 1985. Seasonal variations in natural abundance of ^{15}N in particles sinking to the deep Sargasso Sea. Nature 315, 218–219.

Arthur, M.A., 1979. Paleoceanogrphic events-recognition, resolution, and reconsideration. Rev. Geophys. 17, 1474–1494.

Aubert, O., Droxler, A.W., 1992. General Cenozoic evolution of the Maldives carbonate system (equatorial Indian Ocean). Bull. Cent. Rech. Explor. Prod. Elf-Aquitaine 16, 113–136.

Berner, R.A., Lasaga, A.C., Garrels, R.M., 1983. The carbonate-silicate geochemical cycle and its effect on atmospheric carbon dioxide over the past 100 million years. Am. J. Sci. 283, 641–683.

Betzler, C., Eberli, G.P., Alvarez Zarikian, C.A., Scientists, E., 2017. Site U1468. In: Proceedings of the International Ocean Discovery Program, vol. 359. IODP, College Station. publications.iodp.org.

Betzler, C., Eberli, G.P., Kroon, D., Wright, J.D., Swart, P.K., Nath, B.N., Alvarez-Zarikian, C.A., Alonso-García, M., Bialik, O.M., Blättler, C.L., Guo, J.A., Haffen, S., Horozal, S., Inoue, M., Jovane, L., Lanci, L., Laya, J.C., Mee, A.L.H., Lüdmann, T., Nakakuni, M., Niino, K., Petruny, L.M., Pratiwi, S.D., Reijmer, J.J.G., Reolid, J., Slagle, A.L., Sloss, C.R., Su, X., Yao, Z., Young, J.R., 2016a. The abrupt onset of the modern South Asian Monsoon winds. Sci. Rep. 6, 29838.

Betzler, C., Eberli, G.P., Lüdmann, T., Reolid, J., Kroon, D., Reijmer, J.J.G., Swart, P.K., Wright, J., Young, J.R., Alvarez-Zarikian, C., Alonso-García, M., Bialik, O.M., Blättler, C.L., Guo, J.A., Haffen, S., Horozal, S., Inoue, M., Jovane, L., Lanci, L., Laya, J.C., Hui Mee, A.L., Nakakuni, M., Nath, B.N., Niino, K., Petruny, L.M., Pratiwi, S.D., Slagle, A.L., Sloss, C.R., Su, X., Yao, Z., 2018. Refinement of Miocene sea level and monsoon events from the sedimentary archive of the Maldives (Indian Ocean). Prog. Earth Planet. Sci. 5, 5.

Betzler, C., Eberli, G.P., Zarkian, C., Shipboard Scientific Party, 2016b. Proceedings of the Initial Results of Expedition 359. IODP, College Station.

Bohacs, K.M., 2005. Production, destruction, and dilution-the many paths to source-rock development. In: The Deposition of Organic-Carbon-Rich Sediments: Models, Mechanisms, and Consequences. Society for Sedimentary Geology, Tulsa, pp. 17–33.

Boyle, E.A., 1981. Cadmium, zinc, copper, and barium in foraminifera tests. Earth Planet. Sci. Lett. 53, 11–35.

Brumsack, H.J., 1989. Geochemistry of recent TOC-rich sediments from the Gulf of California and the Black Sea. Geol. Rundsch. 78, 851–882.

Brumsack, H.J., 2006. The trace metal content of recent organic carbon-rich sediments: implications for Cretaceous black shale formation. Palaeogeogr. Palaeoclimatol. Palaeoecol. 232, 344–361.

Coplen, T.B., Brand, W.A., Gehre, M., Groning, M., Meijer, H.A.J., Toman, B., Verkouteren, R.M., 2006. After two decades a second anchor for the VPDB $\delta^{13}C$ scale. Rapid Commun. Mass Spectrom. 20, 3165–3166.

Cranwell, P.A., 1974. Monocarboxylic acis in lake sediments-indicators derived from terrestrial and aquatic biota of paleoenvironmental trophic levels. Chem. Geol. 14, 1–14.

Duncan, R.A., Hargraves, R.B., 1990. $^{40}Ar/^{39}Ar$ geochronology of basement rocks from the Mascarene Plateau, the Chagos Bank, and the Maldives ridge. In: Duncan, R.A., Backman, J., Peterson, L.C. (Eds.), Proceedings of the Ocean Drilling Program, Scientific Results. Ocean Drilling Program, College Station, pp. 43–51.

Emeis, K.-C., Weissert, H., 2009. Tethyan–Mediterranean organic carbon-rich sediments from Mesozoic black shales to sapropels. Sedimentology 56, 247–266.

Francois, R., 1988. A study on the resultation of the concentrations of some trace-metals (Rb, Sr, Zn, Pb, Cu, V, Cr, Ni, Mn, and Mo) in Saanich Inlet sediments, Britich Columbia, Canada. Mar. Geol. 83, 285–308.

Gardner, R.D., Pope, M.C., Wehner, M.P., Donovan, A.D., 2013. Comparative stratigraphy of the Eagle Ford group strata in Lozier Canyon and Antoniio Creek, Terrell County, Texas. Gulf Coast Assoc. Geol. Soc. J. 2, 42–52.

Govindaraju, K., 1994. 1994 compilation of working values and sample description for 383 geostandards. Geostand. Geoanal. Res. 18, 1–158.

Hodell, D.A., Woodruff, F., 1994. Variations on the strontium isotopic ratio of seawater during the Miocene-Stratigraphic and geochemical inplications. Paleoceanography 9, 405–426.

Ishiwatari, R., Yamamoto, S., Shinoyama, S., 2006. Lignin and fatty acid records in Lake Baikal sediments over the last 130 kyr: a comparison with pollen records. Org. Geochem. 37, 1787–1802.

Jenkyns, H.C., 2010. Geochemistry of oceanic anoxic events. Geochem. Geophys. Geosyst. 11.

Knapp, A.N., Hastings, M.G., Sigman, D.M., Lipschultz, F., Galloway, J.N., 2010. The flux and isotopic composition of reduced and total nitrogen in Bermuda rain. Mar. Chem. 120, 83–89.

Koster, J., Wehner, H., Hufnagel, H., 1988. Organic geochemistry and organic petrology of organic-rich sediments within the main dolomite formation (Triassic, Nornian) of the northern calcreous Alps. Org. Geochem. 13, 377–386.

Kunkelova, T., Jung, S.J.A., de Leau, E.S., Odling, N., Thomas, A.L., Betzler, C., Eberli, G.P., Alvarez-Zarikian, C.A., Alonso-García, M., Bialik, O.M., Blättler, C.L., Guo, J.A., Haffen, S., Horozal, S., Mee, A.L.H., Inoue, M., Jovane, L., Lanci, L., Laya, J.C., Lüdmann, T., Bejugam, N.N., Nakakuni, M., Niino, K., Petruny, L.M., Pratiwi, S.D., Reijmer, J.J.G., Reolid, J., Slagle, A.L., Sloss, C.R., Su, X., Swart, P.K., Wright, J.D., Yao, Z., Young, J.R., Lindhorst, S., Stainbank, S., Rueggeberg, A., Spezzaferri, S., Carrasqueira, I., Hu, S., Kroon, D., 2018. A two million year record of low-latitude aridity linked to continental weathering from the Maldives. Prog. Earth Planet. Sci. 5, 86.

Lea, D.W., Boyle, E.A., 1991. Barium in planktonic foraminifera. Geochim. Cosmochim. Acta 55, 3321–3331.

Liebrand, D., de Bakker, A.T.M., Beddow, H.M., Wilson, P.A., Bohaty, S.M., Ruessink, G., Palike, H., Batenburg, S.J., Hilgen, F.J., Hodell, D.A., Huck, C.E., Kroon, D., Raffi, I., Saes, M.J.M., van Dijk, A.E., Lourens, L.J., 2017. Evolution of the early Antarctic ice ages. Proc. Natl. Acad. Sci. USA 114, 3867–3872.

Lyle, M., Backman, J. (Eds.), 2013. Data Report: Calibration of XRF-Estimated $CaCO_3$ Along the Site U1338 Splice. Proceedings of the Integrated Ocean Drilling Program, vol. 320/321. IODP, College Station.

Lyons, T.W., 1991. Upper Holocene sediments of the Black Sea: summary of leg 4 box cores (1988 Black Sea oceanographic expedition). In: Izdar, E., Murray, J.W. (Eds.), Black Sea Oceanography. Kluwer Academic Publishers, Netherlands, pp. 401–441.

Meyers, P.A., Eadie, B.J., 1993. Sources, degradation and recyling of organic matter associated with sinking particles in Lake Michigan. Org. Geochem. 20, 47–56.

Miller, K.G., Mountain, G.S., Wright, J.D., Browning, J.V., 2011. A 180-million-year record of sea level and ice volume variations from continental margin and deep-sea isotopic records. Oceanography 24, 40–53.

Mutti, M., Bernoulli, D., Stille, P., 1997. Temperate carbonate platform drowning linked to Miocene oceanographic events: Maiella platform margin, Italy. Terra Nova 9, 122–125.

Oehlert, A.M., Lamb-Wozniak, K.A., Devlin, Q.B., Mackenzie, G.J., Reijmer, J.J.G., Swart, P.K., 2012. The stable carbon isotopic composition of organic material in platform derived sediments: implications for reconstructing the global carbon cycle. Sedimentology 59, 319–335.

Peterson, L.C., Overpeck, J.T., Kipp, N.G., Imbrie, J., 1991. A high-resolution late quaternary upwelling record from the anoxic Cariaco Basin, Venezuela. Paleoceanography 6, 99–119.

Piper, D.Z., 1974. Rare Earth elements in the sedimentary cycle: a summary. Chem. Geol. 14, 285–304.

Reynolds, R.C., 1963. Matrix correlations in trace element analysis by X-ray fluorescence-Estimation of mass absorption coefficient by compton scattering. Am. Mineral. 48, 1133–1143.

Rossignol-Strick, M., 1985. Mediterranean Quaternary sapropels, an immediate response of the African Monsoon to variation of insolation. Palaeogeogr. Palaeoclimatol. Palaeoecol. 49, 237–263.

Russell, A.D., Morford, J.L., 2001. The behavior of redox-sensitive metals across a laminated–massive–laminated transition in Saanich Inlet, British Columbia. Mar. Geol. 174, 341–354.

Sageman, B.B., Murphy, A.E., Werne, J.P., Straeten, C.A.V., Hollander, D.J., Lyons, T.W., 2003. A tale of shales: the relative roles of production, decomposition, and dilution in the accumulation of organic-rich strata, Middle-Upper Devonian, Appalachian basin. Chem. Geol. 195, 229–273.

Schlanger, S.O., Jenkyns, H.C., 1976. Cretaceous anoxic events: causes and consequences. Geol. Mijnb. 55, 179–184.

Swart, P.K., Oehlert, A.M., Mackenzie, G.J., Eberli, G.P., Reijmer, J.J.G., 2014. The fertilization of the Bahamas by Saharan dust: a trigger for carbonate precipitation? Geology 42, 671–674.

Sweere, T., van den Boorn, S., Dickson, A.J., Reichart, G.J., 2016. Definition of new trace-metal proxies for the controls on organic matter enrichment in marine sediments based on Mn, Co, Mo and Cd concentrations. Chem. Geol. 441, 235–245.

Tribovillard, N., Algeo, T.J., Lyons, T., Riboulleau, A., 2006. Trace metals as paleoredox and paleoproductivity proxies: an update. Chem. Geol. 232, 12–32.

van der Weijden, C.H., Reichart, G.-J., van Os, B.J.H., 2006. Sedimentary trace element records over the last 200 kyr from within and below the northern Arabian Sea oxygen minimum zone. Mar. Geol. 231, 69–88.

Woodruff, F., Savin, S.M., 1989. Miocene deepwater oceanography. Paleoceanography 4, 87–140.

Wright, J., Miller, K., 1992. Miocene stable isotope stratigraphy, site 747, Kerguelan Plateau. In: Schlich, R., Wise Jr., S.W., Palmer-Julson, A. (Eds.), Proceedings of Ocean Drilling Program Scientific Results. College Station, pp. 855–866.

Young, J.R., Archontikis, O., Su, X., Pratiwi, S.D., 2019. Nannofossil palaeoecology of lower Miocene sapropels from IODP Expedition 359, the Maldives. Palaeogeogr. Palaeoclimatol. Palaeoecol. In press.

Zachos, J.C., Pagani, M., Sloan, L., Thomas, E., Billups, K., 2001. Trends, rhythms, and aberrations in global climate 65 Ma to present. Science 292, 686–693.